Molecular Biology of the Cell
Vol. 20, 3471–3480, August 1, 2009

Cisternal Organization of the Endoplasmic Reticulum during Mitosis

Lei Lu,* Mark S. Ladinsky,† and Tom Kirchhausen*

*Department of Cell Biology and Immune Disease Institute, Harvard Medical School, Boston, MA 02115; and †Division of Biology and Howard Hughes Medical Institute, California Institute of Technology, Pasadena, CA 91125

Submitted April 24, 2009; Revised May 21, 2009; Accepted May 26, 2009
Monitoring Editor: Adam Linstedt

The endoplasmic reticulum (ER) of animal cells is a single, dynamic, and continuous membrane network of interconnected cisternae and tubules spread out throughout the cytosol in direct contact with the nuclear envelope. During mitosis, the nuclear envelope undergoes a major rearrangement, as it rapidly partitions its membrane-bound contents into the ER. It is therefore of great interest to determine whether any major transformation in the architecture of the ER also occurs during cell division. We present structural evidence, from rapid, live-cell, three-dimensional imaging with confirmation from high-resolution electron microscopy tomography of samples preserved by high-pressure freezing and freeze substitution, unambiguously showing that from prometaphase to telophase of mammalian cells, most of the ER is organized as extended cisternae, with a very small fraction remaining organized as tubules. In contrast, during interphase, the ER displays the familiar reticular network of convolved cisternae linked to tubules.

INTRODUCTION

The endoplasmic reticulum (ER) of animal cells is a complex membranous network composed of interconnected cisternae or sheets and tubules spread out throughout the cytosol in continuity with the nuclear envelope (Baumann and Walz, 2001; Voeltz *et al*., 2002; Du *et al*., 2004; Shibata *et al*., 2006). During interphase, most of the ER cisternae are located close to the nucleus, whereas the tubules, which are connected to each other by three-way junctions, tend to be located at the cell periphery. During mitosis, the nuclear envelope undergoes a major rearrangement, as it breaks down in part by rapid partition of its membrane-bound contents into the ER (Ellenberg *et al*., 1997; Yang *et al*., 1997; Beaudouin *et al*., 2002). It is of great interest to determine whether any major transformation in the architecture of the ER also occurs during cell division. Such studies are challenging, because of the complex, three-dimensional morphology of the ER and because of the rapidity of the changes in cell organization that accompany cell division. A recent live-cell imaging study, which used the signal peptidase SP12 fused to green fluorescent protein (GFP) to follow ER dynamics during early *Caenorhabditis elegans* embryogenesis, found that the mitotic ER contains extensive, sheet-like structures (Poteryaev *et al*., 2005). A different morphological study, which used electron microscopy to visualize at higher resolution the osmium-stained ER membranes of mitotic HeLa cells, also found that the mitotic ER maintains a cisternal organization; indeed, the electron micrographs show dramatic curvilinear ER tracing within the plane of the section (McCullough and Lucocq, 2005). A more recent attempt to elucidate the organization of the ER during cell division reached the opposite conclusion, however: that the mitotic ER of Chinese hamster ovary (CHO) cells loses its cisternal conformation and becomes completely tubular (Puhka *et al*., 2007). These studies were based on the combined use of live-cell confocal fluorescence imaging and transmission electron microscopy of chemically fixed samples. In an effort to resolve these discrepancies, we have used an improved live-cell imaging approach that is based on spinning disk confocal fluorescence microscopy combined with correction of spherical aberration. This approach permits us to acquire at a suitably high rate three-dimensional (3D) images of relatively thick samples. We have complemented the live-cell imaging with high-resolution information obtained from electron microscopy (EM) tomography of samples preserved by high-pressure freezing and freeze substitution. The results presented here, obtained from four cell types, including CHO cells, unambiguously show that during mitosis most of the ER is organized as an extended array of cisternae, with a few remaining ER tubules associated with the spindle. In contrast, the ER of interphase cells exhibits the characteristic reticular organization, with convolved perinuclear ER cisternae connected to ER tubules present mostly in the cell periphery.

This article was published online ahead of print in *MBC in Press* (http://www.molbiolcell.org/cgi/doi/10.1091/mbc.E09–04–0327) on June 3, 2009.

Address correspondence to: Tom Kirchhausen (kirchhausen@crystal.harvard.edu).

Abbreviations used: GFP, green fluorescent protein; H2B, histone 2B; LBR, lamin B receptor; RFP, red fluorescent protein; Rtn, reticulon.

MATERIALS AND METHODS

Reagents

Nocodazole was purchased from Sigma-Aldrich (St. Louis, MO). *N*-[3-Triethylammoniumpropyl]-4-[*p*-diethylaminophenylhexatrienyl] pyridinium dibromide (FM4-64) and ER Tracker Red were purchased from Invitrogen (Carlsbad, CA). Puromycin was purchased from Calbiochem (San Diego, CA).

Expression plasmids encoding reticulon homology domain of reticulon4a (Rtn4HD) in pAcGFP-C1 (Takara Bio USA, Madison, WI), Sec61β in pAcGFP1-C1 and LBR in pAcGFP-N1 were generous gifts from Tom Rapoport (Harvard Medical School, Boston, MA) (Shibata *et al*., 2008). Histone 2B (H2B)-monomeric red fluorescent protein (mRFP)1 in pBABE-X, ss-GFP-

KDEL in pcDNA, and emerin in pEGFP-N1 (Ostlund *et al*., 1999) were generously provided by Randall King (Harvard Medical School, Boston, MA), Jennifer Lippincott-Schwartz (National Institutes of Health, Bethesda, MD), and Howard Worman (Columbia University, New York, NY), respectively. The expression plasmid encoding cherry-Sec61β was prepared by insertion into the BglII/EcoRI restriction sites of pmCherry-C1 (Takara Bio USA) by direct transfer from Sec61β in pAcGFP1-C1. Expression plasmids encoding cherry-actin and cherry-tubulin were prepared by insertion into the XhoI/BamHI restriction sites of pmCherry-C1 vector by direct transfer from actin-pEGFP and α-tubulin-pEGFP (Takara Bio USA).

Cell Culture and Transfections

HeLa, BSC1, CHO, 293, and normal rat kidney (NRK) cells were cultured in DMEM supplemented in 10% fetal bovine serum. A BSC1 cell line stably expressing GFP-Sec61β was obtained by serial dilution from a pool of stable expressors selected with 0.5 mg/ml Geneticin (G418; Invitrogen) after transfection with Sec61β pAcGFP1-C1; the cell line was maintained in 0.1 mg/ml G418. Transient expression in HeLa, CHO, and 293 cells was done with Lipofectamine 2000 (Invitrogen); 3 h after transfection, the cells were replated in glass-bottomed Petri dish (no. 1.5 glass) (MatTek, Ashland, MA) with fresh culture medium and allowed to grow for ~20 h before imaging. The mitotic index of BSC1 cells expressing GFP-Sec61β was enriched by keeping a confluent culture for 1 d, followed by replating at 70% density, and imaging ~20 h later (Boucrot and Kirchhausen, 2007).

Fluorescence Microscopy

Cells were plated onto glass-bottomed Petri dish (MatTek) and incubated with CO_2 independent medium (Invitrogen) supplemented with 10% fetal bovine serum and 2.5 mM L-glutamine. The Petri dish was placed in an enclosed environment (100% humidity) located on the microscope stage kept at 37°C. Images were acquired with an inverted and fully motorized computer-controlled microscope (Axiovert 200 M; Carl Zeiss, Thornwood, NY) by using a 1.4 numerical aperture (NA) plan-apochromatic 63× objective (Carl Zeiss). The axial position of the sample was controlled with a piezo-driven stage (Applied Scientific Instrumentation, Eugene, OR). The microscope is equipped with a spinning disk confocal head (CSU22; Yokogawa Electric, Tokyo, Japan) linked to a computer-controlled spherical aberration correction device (Infinity Photo-Optical, Boulder, CO) that introduces a 1.5× magnification of the image. The spherical aberration correction device corrects the spherical aberration introduced by the refractive index mismatch between the cell and the glass optics leading to a tightening of the optical point spread function and enhancement in the spatial resolution along the *z*-axis (Saffarian and Kirchhausen, 2008). The resulting increase in signal-to-noise ratio also allows for shorter exposures and decrease in phototoxicity. Data were collected with an EMCCD camera (Cascade 512B; Photometrics, Tucson, AZ) with a total of 172× magnification; under this configuration, each pixel represents 0.093 × 0.093 μm. Images are presented with $\gamma = 1$ unless otherwise indicated in the figure legends. The illumination was achieved using solid-state 40-mW lasers with emissions of 473 and 561 nm and data for each channel was acquired sequentially. The imaging system is under control of Slidebook 4.0 software (Intelligent Imaging Innovations, Denver, CO).

3D image z-stacks were obtained by acquiring sequential optical planes spaced 0.091 μm (or 0.13 μm before correction for the axial distortion, see below). This value (0.13 μm) was calculated using the Nyquist Calculator (http://support.svi.nl/wiki/NyquistCalculator; Scientific Volume Imaging, Hilversum, The Netherlands). For a typical experiment, we acquired ~70 or ~200 sections for a cell imaged during interphase or mitosis, using 20- to 100-ms exposure per channel and a total cycle of 170–290 ms per optical section. Faster or slower acquisition cycles, ranging between 40 and 500 ms per optical section, did not modify the appearance and continuity of the ER patterns. All of the 3D images presented in this article were subjected to image restoration by constrained iterative deconvolution using Huygens Essential version 3.3 (Scientific Volume Imaging). Three-dimensional images were exported as 16-bit TIFF images and deconvolved with the following parameters: x, y, and z sample size, 93, 93, and 130 nm, respectively; theoretical PSF; Nipkow spinning disk; back projected pinhole diameter, 207 nm; back projected pinhole distance, 2.10 μm; lens objective NA, 1.4; optical refractive index, 1.52; sample refractive index, 1.33; excitation wavelength, 473 or 561 nm; emission wavelength, 520 or 590 nm; algorithm, classical maximum likelihood estimation; iteration number, 30; quality threshold, 0.1; photobleaching correction, off; brick layout, auto; signal-to-noise ratio, 20; and background, lowest. We used detailed visual inspection to strictly verify that the deconvolution process did not change the outline or the topology of the ER by direct comparison with the raw image that had not been subjected to deconvolution (Supplemental Figure 5 and Supplemental Movie 1). The 3D image z-stacks shown in Figure 2 and Supplemental Figure 1 are representative of stacks obtained from HeLa cells expressing GFP-Sec61β (59 independent cells during interphase and 77 independent cells during metaphase), HeLa cells expressing ss-GFP-KDEL (3 during interphase and 3 during metaphase), BSC1 cells expressing GFP-Sec61β (58 during interphase and 25 during metaphase), CHO cells expressing GFP-Sec61β (3 during interphase and 11 during metaphase), and CHO cells expressing ss-GFP-KDEL (3 during interphase and 13 during metaphase).

The refractive index mismatch between the glass optics and the sample distorts the image and generates an apparent elongation along the z-optical axis (Ferko *et al*., 2006). This axial correction value (0.70) was obtained according to the procedure of Ferko *et al*. (2006) by using the spinning disk confocal with the spherical aberration correction device to image fluorescent spherical polystyrene beads of 15 μm in diameter (Invitrogen).

Slidebook was used to determine the Pearson's r (R) between the images in two channels in 3D and ImageJ (plugin JACoP; National Institutes of Health) was used to generate the corresponding scatter plots. 3D rendering was done using the HR Rendering module of Volocity version 2.6.3 (Improvision, Waltham, MA).Time-lapse movies were acquired in one optical section by using the spinning disk confocal set up. The time series were exported from Slidebook and converted to QuickTime movies.

Rapid Freezing and Freeze-Substitution EM Tomography

Cells were prepared for EM as described previously (Ladinsky *et al*., 2002), with certain modifications. In brief, cells were grown to confluence on synthetic sapphire disks (3.0 mm in diameter, 0.07 mm in thickness; Rudolf Brügger, Minusio, Switzerland) that were carbon-coated, glow-discharged, and UV-sterilized before use. Disks were rinsed briefly in hexadecene (external cryoprotectant), placed between two aluminum planchettes, and rapidly frozen in a HPM-010 high-pressure freezer (Bal-Tec, Balzers, Leichtenstein). The vitrified samples were freeze-substituted into acetone containing 2% OsO_4 at −75°C for 5 d, warmed to −20°C for 24 h, and then brought to 4°C over 1 h. The disks were rinsed three times with cold acetone, infiltrated with Epon-Araldite resin (Electron Microscopy Sciences, Port Washington, PA), and flat-embedded between a glass slide and a plastic coverslip. After polymerization of the resin (60°C for 48 h), individual interphase or mitotic cells were selected using a phase-contrast light microscope, excised from the resin block, and remounted en face onto plastic sectioning stubs with a two-part epoxy adhesive (Epoxy 907; Miller-Stephenson Chemical, Danbury, CT.). Semithick (200-nm) sections were cut with an UltraCut-UCT microtome (Leica, Vienna, Austria) by using a diamond knife (Diatome, Biel, Switzerland). Sections were transferred to Formvar-coated copper-rhodium slot EM grids (Electron Microscopy Sciences) and stained with uranyl acetate and lead citrate. Colloidal gold particles (10 or 15 nm in diameter; British Biocell International) were placed on both surfaces of the grid to serve as fiducial markers for subsequent image alignment. Sections were imaged with a Tecnai F20 FEG TEM (FEI, Eindhoven, Netherlands) operating at 200 K eV, and images were recorded digitally with a 4 k × 4 k charge-coupled device camera (Gatan, Pleasanton, CA). Dual-axis tilt-series data sets were acquired as described previously (Mastronarde, 1997) using the SerialEM software package (Mastronarde, 2005). Tomographic reconstructions were calculated, analyzed, and segmented using the IMOD software package (Kremer *et al*., 1996) on a Macintosh G5 computer (Apple Computer, Cupertino, CA.). The number of ribosomes associated with a given ER membrane was determined by first combining 15 consecutive 1.1-nm tomographic slices into a single view using the "Slicer" tool in the IMOD software package. This increased the contrast of the membrane profiles and made it easier to select direct bound ribosomes. Bound ribosomes were modeled as individual colored points and counted in each data set. The ribosome density was expressed as the total number of points normalized to the surface area of the traced ER membrane.

Cell Fixation

Cells plated on glass-bottomed Petri dish were first rinsed with phosphate-buffered saline (PBS) and then fixed for 20 min at room temperature by incubation with 2 ml of 4% paraformaldehyde dissolved in PBS or 2% glutaraldehyde in 0.1 M sodium cacodylate buffer, pH 7.4. Cells were imaged in PBS after washing with PBS for three times.

RESULTS

The ER Structure Changes during Cell Division

To analyze the organization of the ER during different stages of cell division, we used live-cell fluorescence imaging with a spinning disk confocal microscope to acquire rapid successions of 3D image stacks from sequential optical planes spaced 0.091 μm apart and extending through the complete cell volume. The fluorescent images in Figure 1 are from different stages during the cell cycle of HeLa cells, in which the ER membranes and nuclear envelope have been labeled by expression of the membrane-bound translocon subunit GFP-Sec61β (green), and in which chromatin has been labeled by expression of the nucleosome subunit H2B-mRFP (red). The images are equatorial optical sections at about the midplane of the cell (Figure 1, a–c4, middle sections) and

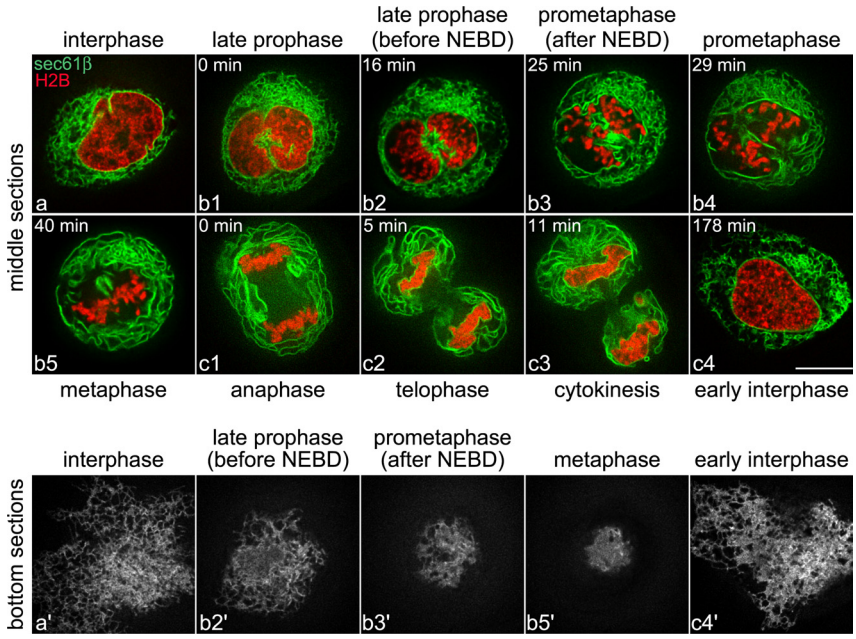

Figure 1. Changes in appearance of the ER during cell division. Spinning disk confocal fluorescence images of live HeLa cells at different stages during the cell cycle; the ER and chromatin are marked by expression of GFP-Sec61β (green) and H2B-mRFP (red), respectively. The upper two rows correspond to equatorial middle sections; the bottom row is from a section adjacent to the glass coverslip. (a and a′) HeLa cell during interphase. (b1–b5 and b2′–b5′) Sequential images from a second HeLa cell starting with late prophase and ending with metaphase. (c1–c4) Sequential images from a third HeLa cell starting with anaphase and ending, after abscission, with early interphase; the images in c4 and c4′ correspond to one of the daughter cells depicted in c3. NEBD, nuclear envelope breakdown. Bar, 10 μm.

sections at a plane adjacent to the plasma membrane in contact with the glass coverslip (Figure 1, a′–c4′, bottom sections). The appearance of the ER is reticular during interphase. There are relatively short, highly branched profiles continuous with the nuclear envelope (Figure 1A). In contrast, during mitosis the appearance of the ER is dominated by long and loosely interconnected curvilinear profiles, 3–10 μm in length; this dramatic change begins in late prophase and continues throughout the remainder of mitosis (Figure 1, b1–c3; also see Supplemental Movie 2 for the time-lapse of ER morphology during mitosis). Gradual recovery of a reticular appearance occurs after abscission (Figure 1, c4 and c4′). The confocal views from the same cells imaged close to the glass coverslip highlight the presence of an extended and prominent ER tubular network during interphase (Figure 1A′), its conversion into extended sheets during mitosis (Figure 1, b2′–b5′), and gradual recovery of a tubular morphology as cells proceed through early stages of interphase (Figure 1, c4 and c4′). As expected, the progressive nuclear envelope breakdown starts at late prophase, followed by its reappearance during anaphase and telophase.

Reticular Architecture of the Interphase ER

To obtain a more detailed understanding of ER organization, we analyzed complete 3D z-stacks from HeLa cells expressing GFP-Sec61β (Figure 2). The fluorescence images correspond to enlarged examples from the juxtanuclear (Figure 2Af) and peripheral regions (Figure 2Ag) depicted every third optical plane, spaced 0.273 μm apart; the corresponding 3D renditions, however, were calculated and drawn using the full set of optical sections spaced 0.091 μm apart (Figure 2A, f′ and g′). The juxtanuclear region contains a characteristic network of highly convolved cisternae, which are conspicuously absent in the peripheral regions; instead, the peripheral ER is made up primarily of a network of long tubules typically linked by three-way junctions (Figure 2Ag) similar to the tubular network present throughout the bottom region of the cell immediately adjacent to the glass coverslip (Figure 1, bottom sections). Similar results were obtained from live-cell 3D imaging of BSC1 and CHO cells expressing GFP-Sec61β (Supplemental Figure 1, A and C), from HeLa and BSC1 cells in which the ER was labeled with ER Tracker Red (Supplemental Figure 2, A and B) and from HeLa and CHO cells expressing ss-GFP-KDEL (Supplemental Figure 1, E and G) used to label the ER (Altan-Bonnet *et al*., 2006).

The Mitotic ER Is Composed Primarily of Extended Cisternae

Without exception, the equatorial views of all cells undergoing mitosis show widespread ER curvilinear profiles with extensive continuity along the plane of observation (Figure 2B). Such curvilinear profiles could only be compatible with a tubular array if they were organized as tubules strictly coplanar with the optical section; as shown below, this is clearly not the case. We find that the curvilinear profiles correspond to the optical sections of a network predominantly composed of relatively loose and extensive ER cisternae. Indeed, inspection of the 3D z-stack obtained from mitotic cells reveals that the curvilinear profiles have extended continuity along the *z*-axis (Figure 2B, a–e, for HeLa cells; see Supplemental Figure 1, B and D, for BSC1 and CHO cells, respectively). The continuity can be seen by inspection of the pattern of fluorescence in every third optical section in the z-stack (Figure 2Bf) or in the corresponding 3D rendering (Figure 2Bf′). The polygonal ER network, which is prominent in the peripheral and bottom regions of interphase cells, is completely absent during metaphase. As observed previously, most of the ER is excluded from the spindle region (Jesch *et al*., 2001), whereas a fraction of the cisternal ER is located close to the spindle poles (Waterman-Storer *et al*., 1993; Terasaki, 2000) (Figure 3). A characteristic layer of extended ER cisternae or sheets also follow the outline of the plasma membrane as detected previously by electron microscopy (McCullough and Lucocq, 2005). This packing of sheets is illustrated by the parallel distributions of GFP-Sec61β and the lipid dye FM4-64, which labels the plasma membrane, and by the distributions of GFP-Sec61β and cherry-actin, which labels the cortical actin layer immediately beneath the plasma membrane (Supplemental Figure 2C).

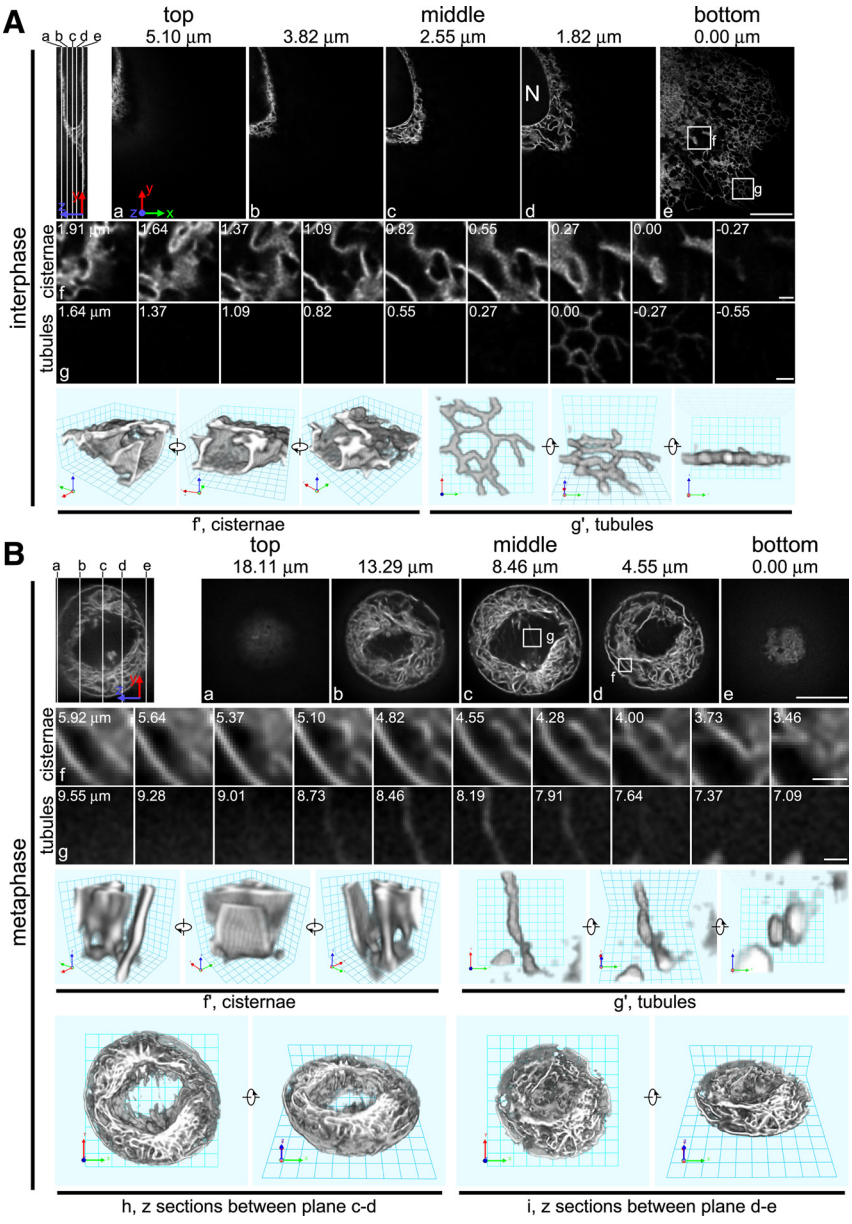

Figure 2. Comparison of ER organization in interphase and metaphase. Sequential spinning disk confocal sections along the *z*-axis and 3D renderings of live-cell images acquired from HeLa cells expressing GFP-Sec61β. (A) HeLa cell imaged during interphase. Top left, planes a–e selected for display in the subsequent panels, with plane e closest to the coverslip. Sequences f and g are from the regions boxed in e; they display every third plane from the sequential acquisition along the *z*-axis; their absolute position is indicated in micrometers. (f′ and g′) are parts of the full z-stack in 3D rendering; they correspond to regions f and g, respectively; their orientations are presented with respect to the coordinate frame in a (the same scheme is followed throughout this article). Bar, 10 μm (e) and 1 μm (f and g). N, nucleus. (B) HeLa cell imaged during metaphase. Top left, planes a–e selected for display. Note that the cell has rounded up and is therefore much thicker than the cell in A. Sequences f and g are from the boxed region in d and c, respectively; they display every third plane from the sequential acquisition along the *z*-axis; their absolute position is indicated in micrometers. The intensity was rescaled in g to help highlight the ER tubules. f′ and g′ are parts of the full z-stack in 3D rendering; they correspond to regions f and g, respectively. Renderings (h and i) show the full z-stack in the middle of the cell, between planes c and d, and between planes d and e, respectively; see Supplemental Movies 11 and 12 for the interactive QTVR movies. Bar, 10 μm (e) and 1 μm (f and g).

We also found extended ER cisternae and notable absence of tubular ER networks in anaphase and telophase HeLa cells (Supplemental Figure 2D) and of various cell types: BSC1 (Supplemental Figure 1B), CHO (Supplemental Figure 1D), and 293 (Supplemental Figure 2E) cells, all expressing GFP-Sec61β; HeLa (Supplemental Figure 1F) and CHO (Supplemental Figure 1H) cells expressing ss-GFP-KDEL; and HeLa and BSC1 cells in which the ER was labeled with ER Tracker Red (Supplemental Figure 2, A and B). We have extended our live-cell imaging analysis to study the distribution of proteins that are normally found in association with the nuclear membrane, and we find that during mitosis, lamin B receptor (LBR) and emerin, two inner nuclear membrane proteins, also occur in the extended ER cisternae with a distribution that closely follows Sec61β; in these cases, the Pearson's correlation coefficients have values of 0.93 and 0.94, respectively (Figure 4).

The extended ER pattern that is prominent throughout the cytosol of the mitotic cells is largely excluded from the central zone that contains the mitotic spindles and chromosomes of HeLa (Jesch *et al*., 2001; McCullough and Lucocq, 2005), BSC1 and CHO cells (Figure 2Bh and Supplemental Figure 1, B and D, respectively). In this region, the detectable ER show up as a limited number of tubules emanating from the spindle poles (e.g., a mean of 9 ± 8 [mean ± SD; n = 13] tubules in HeLa cells, Figure 2Bc; also see Figure 3); these tubules represent ~0.1 ± 0.2% (mean ± SD; n = 7) of the total ER GFP-Sec61β signal in the mitotic cell, as determined by their relative integrated fluorescence intensity. In contrast to the tubular ER network observed during interphase, the less abundant mitotic ER tubules seldom form three-way junctions (except in CHO cells where they are still present; Supplemental Figure 1, D and H, g and g′); they run along spindle microtubules labeled by expression of cherry-tubulin (Figure 3).

We obtained further confirmation of the loss of tubular ER during mitosis by following the ER distribution of reticulons using reticulon homology domain of reticulon4a (Rtn4HD)

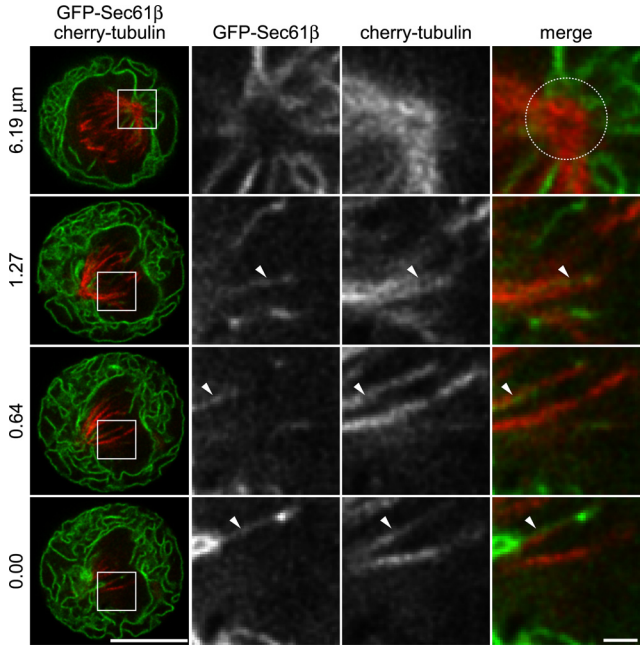

Figure 3. Partial alignment of ER tubules with the spindle in mitotic cells. Sequential spinning disk confocal, live-cell images of a HeLa cell expressing GFP-Sec61β (green) and cherry-tubulin (red) to illustrate the partial association of mitotic ER tubules with microtubules of the spindle (see arrowheads in the enlarged views). Most of the ER tubules are in the central zone of the cell; they seem to radiate from the spindle poles positioned in different sections of the z-stack. A fraction of the ER cisternae converge onto the spindle pole (dotted circle). The intensity in the enlarged views of GFP-Sec61β was rescaled to help highlight the ER tubules. Bars, 10 μm (left column) or 1 μm (enlarged views).

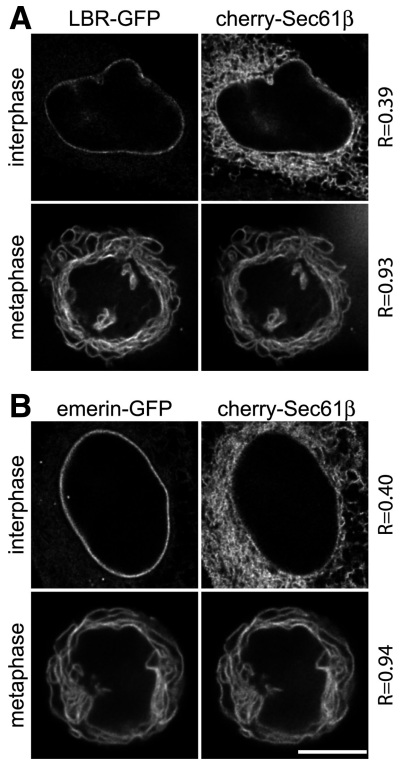

Figure 4. Uniform redistribution of inner nuclear membrane proteins throughout the ER cisternae in mitosis. Optical sections from a 3D z-stack of HeLa cells expressing either (A) LBR-GFP or (B) emerin-GFP together with cherry-Sec61β and imaged during interphase or metaphase. The Pearson's r (R) was used to estimate the extent of colocalization between LBR-GFP or emerin-GFP and cherry-Sec61β and was calculated using the complete 3D image z-stack, which encompassed the entire volume of the cells examined. Bar, 10 μm.

(Shibata *et al*., 2008). As shown previously by others, GFP-Rtn4HD is significantly enriched during interphase in highly curved regions of the ER such as the tubules and the edges of the cisternae; it is much less abundant in the flatter portions of the ER cisternae and in the nuclear envelope (Voeltz *et al*., 2006; Hu *et al*., 2008; Shibata *et al*., 2008) (Figure 5A). As a result, the overall Pearson's r is relatively low: 0.83 $\pm$ 0.02 (mean $\pm$ SD; n = 3) for the 3D colocalization of GFP-Rtn4HD and cherry-Sec61β. In contrast, during mitosis, when an extended cisternal ER has largely replaced the tubular ER, the asymmetric distribution of GFP-Rtn4HD disappears, and there is nearly full colocalization throughout the ER of GFP-Rtn4HD and cherry-Sec61β, with a very high Pearson's r of 0.94 $\pm$ 0.02 (mean $\pm$ SD; n = 3) for metaphase (Figure 5B) and 0.91 $\pm$ 0.05 (mean $\pm$ SD; n = 3) for late anaphase (data not shown); the reformed nuclear envelope lacks Rtn4HD and was excluded from these calculations. The extent of this colocalization continues throughout telophase.

We have used high-resolution EM tomography to confirm the predominantly cisternal structure of the mitotic ER. BSC1 cells were prepared by high-pressure rapid freezing followed by freeze substitution fixation. We identified metaphase cells by the alignment of the condensed chromosomes in the middle of the cell (Figure 6, a and c, and Supplemental Figure 1I). Thick (200-nm) sections were imaged by acquiring tilted views spanning 120° at 1° intervals, which were subsequently aligned and back-projected. Typical examples of the resulting tomographic reconstructions are shown in Figure 6 (b, one cell; d and e, another cell) and Supplemental Figure 1I (a third cell). These images correspond to slices 1.1 nm in thickness and show several membrane profiles (Supplemental Movies 3–6). ER membranes were identified by the presence of ribosomes on their surfaces; we were unable to detect ribosome-free membrane profiles in direct continuity with bona fide ER membranes. Figure 6 also shows several views of the resulting 3D model from one of the reconstructions composed of 4 consecutive 200-nm sections, which was obtained by tracing the membrane profiles in each slice of the reconstruction (Figure 6, f–h; also see Supplemental Movie 4). Analysis of the tomographic data, aided by rendered 3D models, shows metaphase ER composed primarily of extended cisternae with a notable absence of freestanding tubules (see Supplemental Movies 4 and 5). To ensure a reasonable statistical sampling of the mitotic ER, we obtained 23 tomographic reconstructions from 15 different metaphase BSC1 cells, all of which yielded similar results (data not shown). Thus, our high-resolution electron microscopy data confirm the overall cisternal organization of the ER during mitosis, as assessed by live-cell imaging. The density of ribosomes directly associated with mitotic ER membranes is 1000 $\pm$ 300/μm^2 (202 ribosomes counted in 9 cells), whereas it is 1900 $\pm$ 600/μm^2 (374 ribosomes counted in 9 cells) during interphase, in agreement with the trend reported previously using standard EM of chemically fixed cells (Puhka *et al*., 2007).

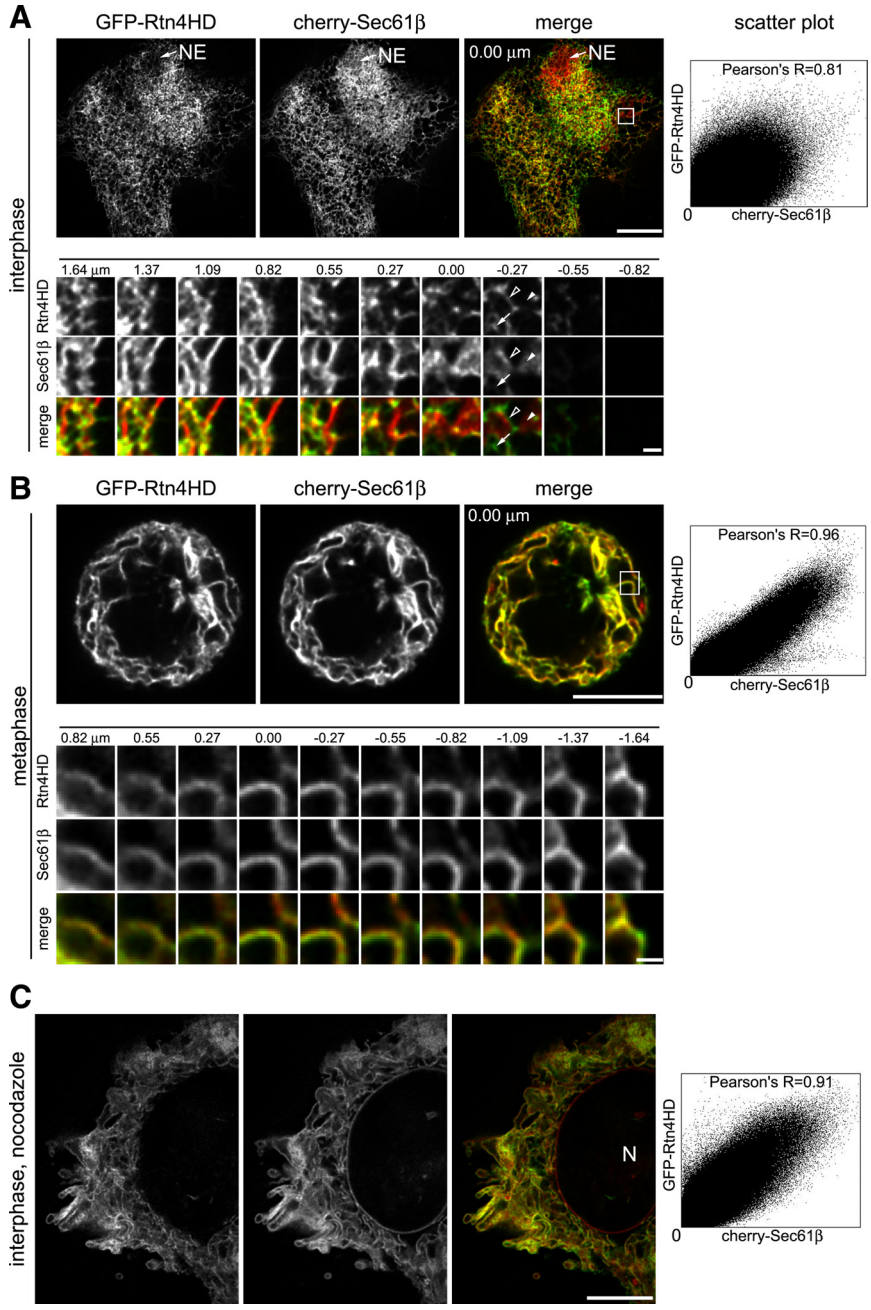

Figure 5. Redistribution of Rtn4HD to the extended ER cisternae. (A) Bottom plane adjacent to the glass coverslip from an interphase HeLa cell expressing GFP-Rtn4HD (green) and cherry-Sec61β (red) obtained using live-cell spinning disk confocal microscopy. The serial sections in the enlarged views are from the boxed region and correspond to every third consecutive plane from the z-stack with their absolute positions along the *z*-axis shown in micrometers. Bar, 1 μm. The section with $z = -0.27$ highlights the preferential location of Rtn4HD to ER regions of high curvature composed of tubules (arrow) and edges of cisternae (empty arrowhead) and its exclusion from flatter regions of the cisternae (solid arrowhead); the nuclear envelope (NE) is devoid of reticulon. Bar, 10 μm. The scatter plot in the right panel shows the extent of colocalization between GFP-Rtn4HD and cherry-Sec61β; the Pearson's r (R) for this cell is 0.81 and 0.83 $\pm$ 0.02 (mean $\pm$ SD) for three cells. These values were calculated using the complete 3D image z-stack, which covered the entire cell volume and the nuclear envelope was not included in these calculations because Rtn4HD is excluded from this region. Bar, 10 μm. (B) Equatorial plane from a metaphase HeLa cell expressing GFP-Rtn4HD (green) and cherry-Sec61β (red) obtained using live-cell spinning disk confocal microscopy; bar, 10 μm. The serial sections in the enlarged views are from the boxed region and correspond to every third consecutive plane from the z-stack with their absolute positions along the *z*-axis shown in micrometers. Bar, 1 μm. The scatter plot in the right panel shows the significantly higher extent of colocalization (than in A) of GFP-Rtn4HD and cherry-Sec61β; the Pearson's r (R) for this cell is 0.96 and 0.94 $\pm$ 0.02 (mean $\pm$ SD) for three cells. (C) Equatorial plane from an interphase HeLa cell expressing GFP-Rtn4HD and cherry-Sec61β treated with 33 μM nocodazole for 2 h. The scatter plot in the right panel shows the significant increase, over the cell panel A, in colocalization of GFP-Rtn4HD and cherry-Sec61β; the Pearson's r (R) for this cell is 0.91. The Pearson's r was calculated using the full z-stack; the nuclear envelope was not included in the calculation. N, nucleus. Bar, 10 μm.

Microtubule Depolymerization Leads to Loss of ER Tubules and Gain of ER Cisternae

It is well established that during cell division, starting with prophase and during mitosis, most of the extended network of microtubules depolymerizes followed by subsequent polymerization to form the spindle microtubules. Recovery of the microtubule cytoskeleton occurs after telophase (Zhai *et al.*, 1996). As described above, we have found that during mitosis most of the ER takes the form of cisternae excluded from the spindle region (Supplemental Figure 3A), with a very small tubular fraction closely associated with spindle microtubules. These observations suggest that microtubules may have a role in generating or stabilizing the tubular organization of the ER. Acute pharmacological disruption of the microtubule cytoskeleton of interphase cells with nocodazole has been reported to cause ER collapse (Terasaki *et al.*, 1986). We have repeated the experiments using live-cell imaging, and we find that the ER collapses by a combination of retraction from the cell periphery and rapid conversion of peripheral tubular ER into extended sheet-like structures, now located throughout the entire cytosol (Figure 7). Loss of peripheral ER tubules and appearance of extended ER cisternae coincide with the onset of microtubule depolymerization within one minute of addition of 33 μM nocodazole to the interphase BSC1 cell (Figure 7A and Supplemental Movie 8) and conversion of ER tubules into cisternae remains even after 3 h of nocodazole treatment; the ER shows curvilinear profiles (single optical sections) and sheet-like structures (3D views) similar in appearance to the ER in mitotic cells (Figure 7B). Similar results were obtained by incubation with lower concentrations of nocodazole (Supplemental Figure 3B). In all these cases, the extended ER

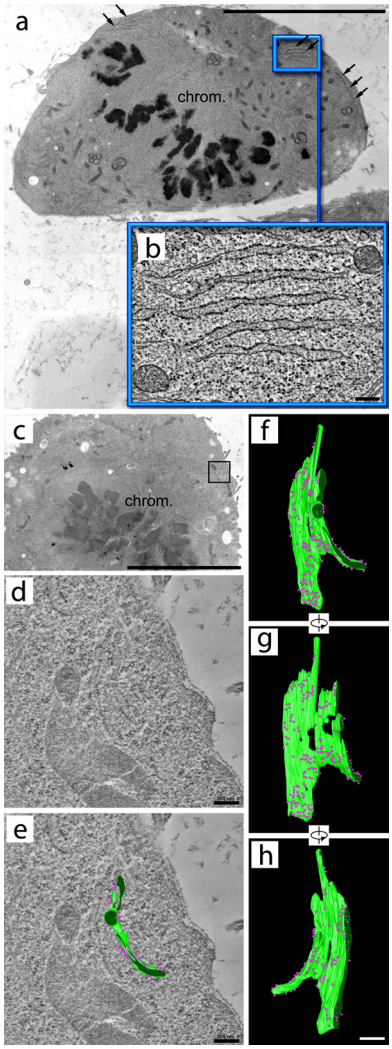

Figure 6. EM tomographic reconstructions from the ER during metaphase. EM tomographic reconstruction from metaphase BSC1 cells prepared by high-pressure freezing and freeze substitution. (a and c) Low-magnification views of different metaphase BSC1 cells identified by their condensed chromosomes (chrom.); examples of curvilinear membrane ER profiles (arrows) are shown in a. Bar, 10 μm. (b) Example, at higher magnification, of a tomographic 1.1-nm slice showing examples of curvilinear membrane profiles, identified as ER by their close association with ribosomes (see Supplemental Movie 3 for the complete set of serial slices spanning ~200 nm that illustrates presence of hollow cisternae and absence of tubules). Bar, 200 nm. (d and e) The reconstruction is composed of four serial 200-nm sections, representing ~800 nm of cellular thickness from the boxed region in c; see Supplemental Movie 4 for the complete set of serial slices. Representative tomographic slice of 1.1 nm in thickness without (d) and with (e) superimposition of the model contour tracing of the ER membrane. Identity of the ER membrane (green) was established by the presence of ribosomes (magenta) adhering to its cytosolic surface. Bar, 200 nm. Panels f–h show three views of the rendered 3D model also depicted in Supplemental Movie 7. The ER in the sample conforms primarily to a cisternal structure; the hollow cisterna is evident in f–h. Bar, 200 nm.

cisternae tend to be aligned parallel to the bottom of the cells. A very small fraction of the ER remains organized as short tubules in the cell periphery (Figure 7B, arrows). The distribution of GFP-Rtn4HD in interphase HeLa (Figure 5C) or BSC1 (data not shown) cells treated with nocodazole likewise mimics what happens in mitotic cells: the segregated distribution of GFP-Rtn4HD and cherry-Sec61β is lost and the two signals now colocalize, with a high Pearson's r, whereas they still remain segregated in the NE. Very high expression of reticulon induces ER tabulation and prevents this nocodazole effect in BSC1 cells (data not shown), in agreement with the stabilization of ER tubules observed in COS7 cells also treated with nocodazole (Shibata *et al*., 2008). Finally, we observed transformation of the reticular ER into extended cisternae in nocodazole treated interphase cells by high-resolution high pressure freezing and freeze substitution electron microscopy (Figure 7C and Supplemental Movie 9). The example shown highlights the cisternal appearance of the ER in the cell periphery, a region that in untreated cells is enriched in ER tubules. All these observations suggest that presence of an organized microtubule cytoskeleton is a major determinant for the presence and/or stability of tubular ER.

In contrast to the observations just described in living cells, we found that the sheet-like appearance of the ER is lost in chemically fixed cells and is replaced by a highly fenestrated structure. To illustrate this point, we used spinning disk fluorescence microscopy to image GFP-Sec61β–expressing HeLa cells during mitosis or during interphase after nocodazole treatment, before and after fixation at room temperature with 4% paraformaldehyde, a standard procedure used for fluorescence microscopy (Supplemental Figure 4, A–C). ER fenestration is less pronounced when fixation is carried out with 2% glutaraldehyde alone (Supplemental Figure 4D) or with a mixture of 1.5% glutaraldehyde and 2% paraformaldehyde (data not shown), the fixation conditions used by Puhka and colleagues. In contrast, inclusion before fixation of puromycin, to mimic the partial release observed during mitosis of ribosomes bound to the ER (Pukha *et al*., 2007), results in extensive ER fenestration even though no detectable effect is observed by live-cell imaging (Supplemental Figure 4D). The evident disruption of the continuous, extended appearance of the ER helps explain previous difficulties in detecting the presence of cisternal ER in chemically fixed interphase cells treated with nocodazole and the putative conversion of ER cisternae into a tubular ER network in puromycin treated cells observed using conventional electron microscopy (Puhka *et al*., 2007).

DISCUSSION

We present structural evidence, from rapid, live-cell, 3D imaging with confirmation from high-resolution EM tomography, to show that during the mitosis of mammalian cells, most of the ER is organized as extended cisternae, with a very small fraction remaining organized as tubules. In contrast, during interphase, the ER displays the familiar reticular network of convolved cisternae linked to tubules.

Several groups, including ours, have used live-cell imaging to follow the distribution of ER and nuclear envelope markers during mitosis. These include the ER markers Sec61β (Anderson and Hetzer, 2007; this work); ss-GFP (or RFP)-KDEL (Terasaki, 2000; Altan-Bonnet *et al*., 2006; this work); β-galactosyltransferase (Terasaki, 2000; Altan-Bonnet *et al*., 2006; this work); reticulon4HD (this work); ER Tracker Red (this work); SP12 (Poteryaev *et al*., 2005), PDI (Bobinnec *et al*., 2003); and the nuclear envelope markers emerin (this work), LBR (Ellenberg *et al*., 1997; this work), and POM121, gp210 (Anderson and Hetzer, 2007). In all cases, the pattern within a single optical section always seems as long, smooth, curvilinear tracings spanning 3 μm or more. What is the interpretation of these patterns? The simplest interpretation

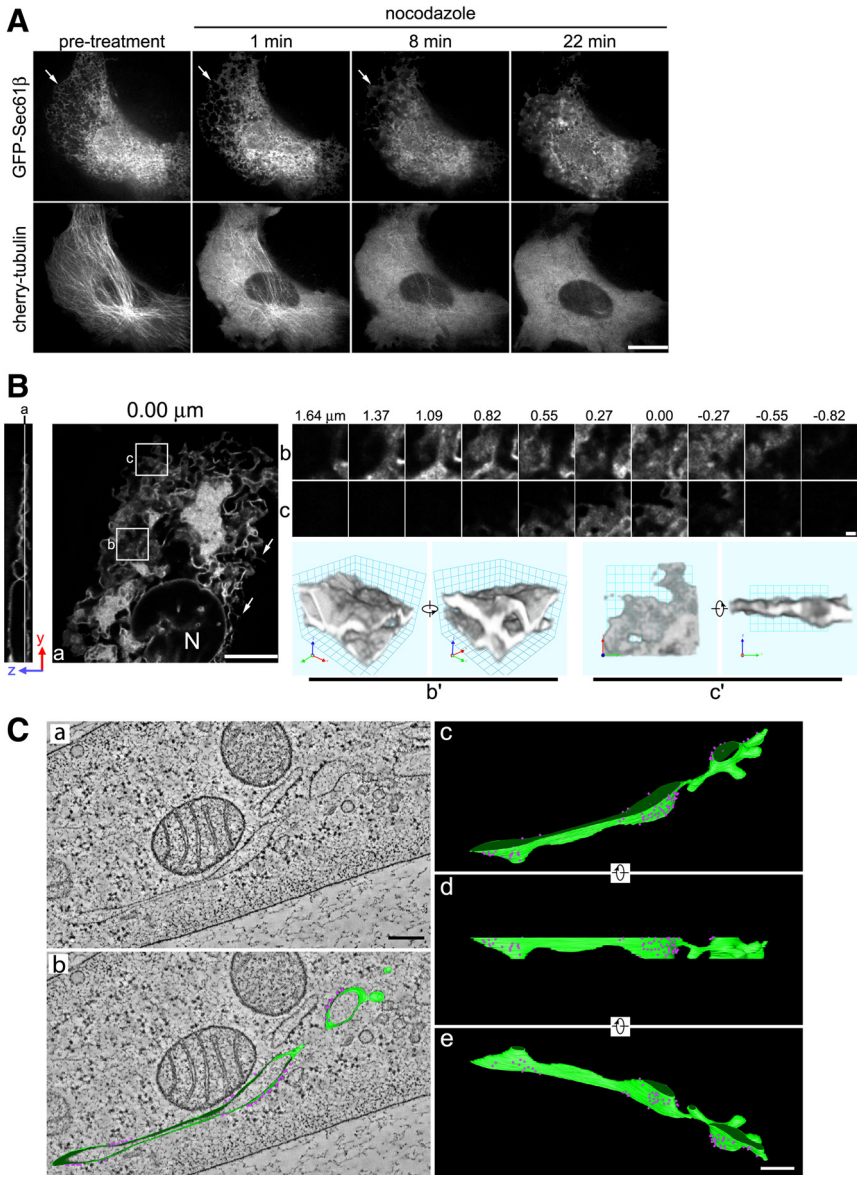

Figure 7. Microtubule depolymerization by nocodazole treatment results in loss of ER tubules and gain of extended ER cisternae. (A) A BSC1 cell expressing GFP-Sec61β (top row) and cherry-tubulin (bottom row) was exposed during interphase to 33 μM nocodazole; the images are from a single-plane, time-lapse series acquired using the spinning disk confocal microscope and correspond to an optical section close to the glass coverslip (see Supplemental Movie 8). The arrows highlight a peripheral region containing tubular ER joined by three-way junctions and its replacement with extended cisternae after microtubule depolymerization. Bar, 10 μm. (B) Spinning disk confocal z-sections and 3D rendering of a BSC1 cell stably expressing GFP-Sec61β imaged during interphase and showing the effects of nocodazole treatment. Left, plane a selected for display. Sequences b and c display enlarged views from the boxed regions in a and correspond to every third plane along the *z*-axis; their absolute position along the *z*-axis is indicated in micrometers. The intensity was rescaled in b and c to help highlight the ER cisternae. Views (b′) and (c′) are 3D renderings of regions b and c, respectively, from the full 3D z-stack. Bar, 10 μm (a) and 1 μm (c). N, nucleus. (C) EM tomographic reconstruction of the ER in an NRK cell treated with nocodazole during interphase. The reconstruction was made from a 200-nm section. Representative tomographic slice of 1.1 nm in thickness without (a) and with (b) superimposition of the contour of a model that traces the ER membrane. Identity of the ER membrane (green) was established by its close association with small particles corresponding to ribosomes (magenta), which cover the cytosolic face of ER cisternae. c–e show three rendered views of the 3D model also depicted in Supplemental Movie 9. Note that a budding domain is present on the right side of the reconstruction. Bars, 200 nm.

is that the curvilinear tracings belong to optical sections of cisternal membranes running at different angles to the view axis, rather that to a meshwork of tubules with a preferential orientation orthogonal to the view axis. To test this hypothesis, we generated 3D views of the cells with a fast visualization protocol specifically designed to obtain finely spaced sequential optical sections. Simple inspection of the 3D stacks shows that in every case, the curvilinear tracings correspond to optical sections of what turns out to be an extended structure rather than to sagittal views of tubules spread in a plane orthogonal to the axis of view. We reached the same conclusion regardless of whether the analysis was done from images restored in 3D by iterative deconvolution or directly from raw, unprocessed images (Supplemental Figure 5, A and B, and Supplemental Movie 1). Our live-cell imaging of mitotic cells is in complete agreement with high resolution EM tomographic observations from mitotic cells showing the absence of tubular ER and presence of cisternae ER.

A recent article proposes an alternative model, suggesting that the ER is completely tubular during mitosis (Puhka *et al*., 2007). This conclusion was reached with data acquired by deconvolution confocal microscopy of live CHO cells expressing the ER markers ss-GFP-KDEL or Hsp47-GFP and by conventional electron microscopy of chemically fixed samples. There are a number of reasons for the different conclusions. 1) We used the full 3D data set for a mitotic cell, typically composed of 200 optical sections spaced 0.091 μm apart, to track the image profiles in 3D. Puhka *et al*. (2007) used only four to five sections per mitotic cell, spaced 5 to 10 sections apart (or 1.43–2.85 μm according to their methods) to generate the data for analysis. Because this procedure necessarily breaks the continuity of any sheet structure, it will artificially generate short profiles and branch points that would lead to an apparent increase in tubular profiles (Supplemental Figure 5C). 2) The cell type or the specific distribution of the GFP-tagged protein used for the experiments might in principle account for the discrepancies. We have, however, repeated the experiments of Puhka *et al*. (2007) to visualize mitotic CHO cells expressing GFP-Sec61β (Supplemental Figure 1D) or ss-GFP-KDEL (Supplemental Figure 1H), and in every case, regardless of the chimeric protein

used, we have found the same curvilinear distribution (on a single optical section) and extended cisternae (by 3D rendering) of these proteins, with only a limited amount of tubular ER. 3) We have used significantly different fixation procedures in preparation for electron microscopy. We used high pressure freezing followed by freeze substitution, a procedure known to minimize alterations in the membrane organization of biological samples. Our tomographic observations clearly show absence of ER tubules and almost exclusive presence of ER cisternae in mitotic cells. In contrast, Puhka and colleagues chemically fixed their samples at room temperature, a procedure known to be more disruptive, and then find tubular ER in their EM tomographic reconstructions. Indeed, as shown here, the conventional chemical fixation clearly modifies the appearance of the ER, which, when visualized by spinning disk confocal fluorescence microscopy, shows loss of continuity and generation of fenestrated ER structures in mitotic cells or in interphase cells treated with nocodazole (Supplemental Figure 4). We also found that puromycin exacerbates ER fenestration in chemically fixed cells but that it has no detectable effect on the ER structure of unfixed cells. These observations indicate that ER tubulation might be an experimental artifact due to chemical fixation of cells, in which the ER has been depleted of attached ribosomes during mitosis or by puromycin treatment. 4) Finally, we note that curvilinear ER profiles, very similar to ours, were observed by fluorescence confocal microscopy during mitosis in developing embryos of *C. elegans*, and analysis of the 3D images led to the conclusion that the ER forms sheets (Poteryaev *et al*., 2005). Therefore, we propose that the ER undergoes a transformation during cell division, from a network of cisternae and tubules characteristic of cells in interphase, to an organization dominated by extended cisternae during mitosis. As these changes occur in the four mammalian cell lines studied here and in *C. elegans* embryos, we believe they are likely to be quite general.

We suggest that the extensive reorganization of the microtubule cytoskeleton during mitosis is a strong determinant of the loss of a tubular ER network and the appearance of extended ER cisternae. The few ER tubules we see in mitotic cells seem to be engaged with spindle microtubules. The rapid, extensive, and reversible loss of tubular ER and the generation of extended ER cisternae upon nocodazole-induced microtubule depolymerization in interphase cells also imply a close connection between the microtubule cytoskeleton and ER architecture (Supplemental Movie 10).

Members of the reticulon and DP1/Yop1p ER-protein families are thought to tubulate ER membranes (Voeltz *et al*., 2006; Hu *et al*., 2008; Shibata *et al*., 2008). It is therefore possible that during mitosis, transient loss of their proposed tubulation function might facilitate the acute loss of tubular ER that we report. This model would have to be reconciled, however, with our observations that simple addition of nocodazole to interphase cells results in the tubular to cisternal ER transformation and that in mitotic cells and in nocodazole-treated interphase cells, Rtn4HD (and presumably other members of the family) relocates throughout the extended ER cisternae. An alternative explanation is that these proteins partition to regions of high curvature and cooperate with more active, cytoskeleton-based mechanisms to stabilize tightly curved ER membranes. Thus, during interphase, the reticulons concentrate at the edges of cisternae and in the tubular regions of the ER (Voeltz *et al*., 2006; this study), whereas during mitosis or in nocodazole-treated interphase cells, when highly curved ER regions are scarce, the reticulons relocate to the more extended portions of the ER.

This new perspective, of a cisternal rather than a tubular ER during mitosis, has important implications for how the ER might contribute to regenerating the nuclear envelope. In particular, it suggests that cisternal, rather than tubular, ER may produce the nuclear envelope, which reforms during the later stages of mitosis and well before the reappearance of ER tubules.

ACKNOWLEDGMENTS

This work is funded by National Institutes of Health grant R01 GM-075252 (to T .K.). We thank Eric Marino for assistance in maintaining the microscope facility in the Kirchhausen laboratory and Tom Rapoport, Randall King, Jennifer Lippincott-Schwartz, and Howard Worman for generously providing reagents.

REFERENCES

Altan-Bonnet, N., Sougrat, R., Liu, W., Snapp, E. L., Ward, T., and Lippincott-Schwartz, J. (2006). Golgi inheritance in mammalian cells is mediated through endoplasmic reticulum export activities. Mol. Biol. Cell *17*, 990–1005.

Anderson, D. J., and Hetzer, M. W. (2007). Nuclear envelope formation by chromatin-mediated reorganization of the endoplasmic reticulum. Nat. Cell Biol. *9*, 1160–1166.

Baumann, O., and Walz, B. (2001). Endoplasmic reticulum of animal cells and its organization into structural and functional domains. Int. Rev. Cytol. *205*, 149–214.

Beaudouin, J., Gerlich, D., Daigle, N., Eils, R., and Ellenberg, J. (2002). Nuclear envelope breakdown proceeds by microtubule-induced tearing of the lamina. Cell *108*, 83–96.

Bobinnec, Y., Marcaillou, C., Morin, X., and Debec, A. (2003). Dynamics of the endoplasmic reticulum during early development of *Drosophila melanogaster*. Cell Motil. Cytoskeleton *54*, 217–225.

Boucrot, E., and Kirchhausen, T. (2007). Endosomal recycling controls plasma membrane area during mitosis. Proc. Natl. Acad. Sci. USA *104*, 7939–7944.

Du, Y., Ferro-Novick, S., and Novick, P. (2004). Dynamics and inheritance of the endoplasmic reticulum. J. Cell Sci. *117*, 2871–2878.

Ellenberg, J., Siggia, E. D., Moreira, J. E., Smith, C. L., Presley, J. F., Worman, H. J., and Lippincott-Schwartz, J. (1997). Nuclear membrane dynamics and reassembly in living cells: targeting of an inner nuclear membrane protein in interphase and mitosis. J. Cell Biol. *138*, 1193–1206.

Ferko, M. C., Patterson, B. W., and Butler, P. J. (2006). High-resolution solid modeling of biological samples imaged with 3D fluorescence microscopy. Microsc. Res. Tech. *69*, 648–655.

Fricker, M., Hollinshead, M., White, N., and Vaux, D. (1997). Interphase nuclei of many mammalian cell types contain deep, dynamic, tubular membrane-bound invaginations of the nuclear envelope. J. Cell Biol. *136*, 531–544.

Hu, J., Shibata, Y., Voss, C., Shemesh, T., Li, Z., Coughlin, M., Kozlov, M. M., Rapoport, T. A., and Prinz, W. A. (2008). Membrane proteins of the endoplasmic reticulum induce high-curvature tubules. Science *319*, 1247–1250.

Jesch, S. A., Mehta, A. J., Velliste, M., Murphy, R. F., and Linstedt, A. D. (2001). Mitotic Golgi is in a dynamic equilibrium between clustered and free vesicles independent of the ER. Traffic *2*, 873–884.

Kremer, J. R., Mastronarde, D. N., and McIntosh, J. R. (1996). Computer visualization of three-dimensional image data using IMOD. J. Struct. Biol. *116*, 71–76.

Ladinsky, M. S., Wu, C. C., McIntosh, S., McIntosh, J. R., and Howell, K. E. (2002). Structure of the Golgi and distribution of reporter molecules at 20 degrees C reveals the complexity of the exit compartments. Mol. Biol. Cell *13*, 2810–2825.

Mastronarde, D. N. (1997). Dual-axis tomography: an approach with alignment methods that preserve resolution. J. Struct. Biol. *120*, 343–352.

Mastronarde, D. N. (2005). Automated electron microscope tomography using robust prediction of specimen movements. J. Struct. Biol. *152*, 36–51.

McCullough, S., and Lucocq, J. (2005). Endoplasmic reticulum positioning and partitioning in mitotic HeLa cells. J. Anat. *206*, 415–425.

Ostlund, C, Ellenberg, J., Hallberg, E., Lippincott-Schwartz, J., and Worman, H. J. (1999). Intracellular trafficking of emerin, the Emery-Dreifuss muscular dystrophy protein. J. Cell Sci. *112*, 1709–1719.

Poteryaev, D., Squirrell, J. M., Campbell, J. M., White, J. G., and Spang, A. (2005). Involvement of the actin cytoskeleton and homotypic membrane fusion in ER dynamics in *Caenorhabditis elegans*. Mol. Biol. Cell *16*, 2139–2153.

Puhka, M., Vihinen, H., Joensuu, M., and Jokitalo, E. (2007). Endoplasmic reticulum remains continuous and undergoes sheet-to-tubule transformation during cell division in mammalian cells. J. Cell Biol. *179*, 895–909.

Saffarian, S., and Kirchhausen, T. (2008). Differential evanescence nanometry: live-cell fluorescence measurements with 10 nm-axial resolution on the plasma membrane. Biophys. J. *94*, 2333–2342.

Shibata, Y., Voeltz, G. K., and Rapoport, T. A. (2006). Rough sheets and smooth tubules. Cell *126*, 435–439.

Shibata, Y., Voss, C., Rist, J. M., Hu, J., Rapoport, T. A., Prinz, W. A., and Voeltz, G. K. (2008). The reticulon and DP1/Yop1p proteins form immobile oligomers in the tubular endoplasmic reticulum. J. Biol. Chem. *283*, 18892–18904.

Terasaki, M., Chen, L. B., and Fujiwara, K. (1986). Microtubules and the endoplasmic reticulum are highly interdependent structures. J. Cell Biol. *103*, 1557–1568.

Terasaki, M. (2000). Dynamics of the endoplasmic reticulum and Golgi apparatus during early sea urchin development. Mol. Biol. Cell *11*, 897–914.

Voeltz, G. K., Rolls, M. M., and Rapoport, T. A. (2002). Structural organization of the endoplasmic reticulum. EMBO Rep. *3*, 944–950.

Voeltz, G. K., Prinz, W. A., Shibata, Y., Rist, J. M., and Rapoport, T. A. (2006). A class of membrane proteins shaping the tubular endoplasmic reticulum. Cell *124*, 573–586.

Waterman-Storer, C. M., Sanger, J. W., and Sanger, J. M. (1993). Dynamics of organelles in the mitotic spindles of living cells: membrane and microtubule interactions. Cell Motil. Cytoskeleton *26*, 19–39.

Yang, L., Guan, T., and Gerace, L. (1997). Integral membrane proteins of the nuclear envelope are dispersed throughout the endoplasmic reticulum during mitosis. J. Cell Biol. *137*, 1199–1210.

Zhai, Y., Kronebusch, P. J., Simon, P. M., and Borisy, G. G. (1996). Microtubule dynamics at the G2/M transition: abrupt breakdown of cytoplasmic microtubules at nuclear envelope breakdown and implications for spindle morphogenesis. J. Cell Biol. *135*, 201–214.